Iron accumulation causes impaired myogenesis correlated with MAPK signaling pathway inhibition by oxidative stress

Yasumasa Ikeda[1*], Akiho Satoh[2*], Yuya Horinouchi[1*], Hirofumi Hamano[4], Hiroaki Watanabe[3], Mizuki Imao[2], Masaki Imanishi[4], Yoshito Zamami[3,4], Kenshi Takechi[5], Yuki Izawa-Ishizawa[1], Licht Miyamoto[2], Tasuku Hirayama[6], Hideko Nagasawa[6], Keisuke Ishizawa[3,4], Ken-ichi Aihara[7], Koichiro Tsuchiya[2], Toshiaki Tamaki[1]

[1]Department of Pharmacology, [2]Department of Medical Pharmacology, [3]Department of Clinical Pharmacology, [7]Department of Community Medicine for Diabetes and Metabolic Disorders, Institute of Biomedical Sciences, Tokushima University Graduate School, Tokushima, Japan

[4]Department of Pharmacy, [5]Clinical Trial Center for Developmental Therapeutics, Tokushima University Hospital, Tokushima, Japan

[6]Laboratory of Pharmaceutical and Medicinal Chemistry, Gifu Pharmaceutical University, Gifu, Japan

*These authors contributed equally to this work.

Corresponding author: Yasumasa Ikeda, MD, PhD

Department of Pharmacology, Institute of Biomedical Sciences, Tokushima University Graduate School,

3-18-15 Kuramoto-cho, Tokushima, 770-8503, Japan

E-mail: yasuike@tokushima-u.ac.jp

Tel: +81-88-633-7061, Fax: +81-88-633-7062

ABBREVIATIONS: CTX, cardiotoxin; MAPKs, mitogen-activated protein kinases; CKD, chronic kidney disease; SFO, saccharated ferric oxide; Myh, myosin heavy chain; FTH, ferritin heavy chain; FTL, ferritin light chain; ERK, extracellular signal-regulated kinase; HPF, Hydroxyphenyl fluorescein; DFO, deferoxamine; GA, gastrocnemius; DAPI, 4′,6-diamidino-2-phenylindole; DHE. dihydroethidium; Col1a1, collagen type I alpha 1 chain; Col1a2, collagen type I alpha 2 chain; Col3a1, collagen type III alpha 1 chain; Tgf-β1, transforming growth factor-beta 1; DCFH-DA, 2′, 7′-dichlorofluorescin diacetate; TBARS, thiobarbituric acid reactive substance ; MDA, malondialdehyde; ROS, reactive oxygen species; NF-κB, nuclear factor-kappa B

1   **Abstract**

2   Skeletal muscle atrophy is caused by disruption in the homeostatic balance of muscle

3   degeneration and regeneration under various pathophysiological conditions. We have

4   previously reported that iron accumulation induces skeletal muscle atrophy via a

5   ubiquitin ligase-dependent pathway. However, the potential effect of iron accumulation

6   on muscle regeneration remains unclear. To examine the effect of iron accumulation on

7   myogenesis, we used a mouse model with cardiotoxin (CTX)-induced muscle

8   regeneration *in vivo* and C2C12 mice myoblast cells *in vitro*. In mice with iron overload,

9   the skeletal muscles exhibited increased oxidative stress and decreased expression of

10   satellite cell markers. Following CTX-induced muscle injury, these mice also displayed

11   delayed muscle regeneration with a decrease in the size of regenerating myofibers,

12   reduced expression of myoblast differentiation markers, and decreased phosphorylation

13   of mitogen-activated protein kinase signaling pathways. *In vitro*, iron overload also

14   suppressed the differentiation of C2C12 myoblast cells, but the suppression could be

15   reversed by superoxide scavenging using tempol. Excess iron inhibits myogenesis via

16   oxidative stress, leading to an imbalance in skeletal muscle homeostasis.

17

18   **Keywords:** iron, myogenesis, oxidative stress, mitogen-activated protein kinases

19   (MAPKs)

Introduction

Iron is an essential trace metal element. However, excess iron causes oxidative stress by catalyzing the production of highly toxic hydroxy-radicals via the Fenton reaction. Disorders, such as cardiomyopathy, hepatic failure, and diabetes, are induced by ectopic accumulation of excess iron in hereditary iron overload disorders (1). Moreover, increased iron content in the body can also be associated with many other diseases that do not fall under the domain of iron overload disorders. These include liver diseases (2), obesity (3), diabetes (4, 5), cardiovascular diseases (6, 7), and kidney diseases (8). These diseases are ameliorated by iron reduction, as shown by both clinical (9-11) and experimental studies (12-16) .

Skeletal muscle wasting, also known as sarcopenia, is caused by aging (17) and chronic disorders, such as chronic heart failure (18), chronic kidney disease (CKD) (19), diabetes (20), and metabolic disease (21), which worsen quality of life and lead to morbidity or mortality (22). In terms of the relationship between skeletal muscle and tissue iron content indicated by serum ferritin (a marker of body iron store), high iron content is associated with a decrease in skeletal muscle mass in elderly women (23). The serum ferritin level is also higher in sarcopenic obese individuals (24). Skeletal muscle mass has been shown to decrease with increased iron accumulation (25-27) due to the alterations in iron metabolism in aged rats. Direct iron administration reduces skeletal muscle mass due to elevated oxidative stress (28), and skeletal muscle atrophy,

40   induced by excessive iron, involves E3 ubiquitin ligase action mediated by the

41   inactivation of Akt-FOXO3a due to oxidative stress (29).

42   Skeletal muscle is a highly regenerative organ in the body. The loss of muscle

43   mass is induced by enhanced muscle degradation and by reduced muscle regeneration

44   (30). In muscle regeneration, satellite cells are crucial in muscle growth and repair. In

45   the process of regeneration upon muscle injury, the behavior of satellite cells is tightly

46   regulated by several transcription factors during quiescence, proliferation, and

47   differentiation. Pax-7 is expressed in adult quiescent satellite cells in mice (31) and

48   human (32). In response to injury, satellite cells proliferate and activated cells express

49   myogenic regulatory factors including myogenic differentiation 1 (*MyoD*), myogenic

50   factor 5 (*Myf5*), and myogenin (*Myog*) (33), and Pax-7 is downregulated prior to

51   terminal differentiation to myofibers (34). Notably, satellite cell dysfunction is seen in

52   mouse models of aging (35, 36), diabetes (37-39), and CKD (40). and satellite cell

53   numbers also decrease with age in humans (32, 41, 42).

54   The balance between muscle regeneration and degradation is important for the

55   maintenance of muscle mass. As described above, excess iron promotes skeletal muscle

56   degradation via activation of E3 ubiquitin ligase (29). However, whether the

57   regenerative potential of normal skeletal muscle is altered during iron overload induced

58   muscle wasting is unknown. In the present study, we found that excess iron

59   accumulation suppressed skeletal muscle differentiation by suppressing the

60   mitogen-activated protein kinase (MAPK) signaling pathway, and that the delay in

4

61 skeletal muscle differentiation was a consequence of oxidative stress induced by excess

62 iron.

63 **Material and methods**

64 *Materials*

65 Saccharated ferric oxide (SFO) and cardiotoxin (CTX) were purchased from

66 Nichi-Iko Pharmaceutical (Toyama, Japan) and A (St Louis, MO, USA), respectively.

67 The following commercially available antibodies were used: anti-myosin heavy chain

68 (Myh) 3 (same as embryonic Myh (eMyh)), anti-myogenin, anti-ferritin heavy chain

69 (FTH), anti-ferritin light chain (FTL) (Santa Cruz Biotechnology, Inc., Dallas, TX),

70 anti-phospho-p38MAPK (Thr180/Tyr182), anti-total p38MAPK, anti-phospho-p44/42

71 MAPK (extracellular signal-regulated kinase 1/2, ERK1/2), anti-total p44/42 MAPK

72 (Extracellular Signal-regulated Kinase (ERK) 1/2) (Cell Signaling Technology,

73 Danvers, MA, USA), anti-Pax-7 (Developmental Studies Hybridoma Bank, Iowa City,

74 IA, USA), and anti-α-tubulin (Merck KGaA, Darmstadt, Germany) as a protein loading

75 control. Hydroxyphenyl fluorescein (HPF) was purchased from Goryo chemical

76 (Sapporo, Japan). Deferoxamine (DFO) was purchased from Sigma-Aldrich (St. Louis,

77 Missouri, USA).

78 *Animal preparation and procedures*

79 All experimental procedures for mice were performed in accordance with the

80 guidelines of the Animal Research Committee of Tokushima University Graduate

81 School, and the protocol was approved by the Institutional Review Board of Tokushima

82 University Graduate School for animal protection (Permit Number: 13095). The mice

83 were randomly divided into two groups: vehicle group and iron treatment group.

84 Seven-week-old male C57BL/6J mice were obtained from Nippon CLEA (Tokyo,

85 Japan) and were maintained with *ad libitum* access to water and food (Type NMF;

86 Oriental Yeast, Tokyo, Japan). After 1 week of acclimation, to prepare a mouse model

87 of iron overload, mice were treated once a week with intraperitoneal SFO (2 mg/200

88 µl/25 g mouse) or with the same volume of vehicle for four consecutive weeks (43).

89 Aged C57BL/6J mice were 2 years old. Control young mice were 2 months old. In the

90 type 2 diabetic mouse model, 8-week-old BKS-background *db/db* mice (diabetes) and

91 heterozygous *db/m* mice (non-diabetes) were purchased from Nippon CLEA Japan, Inc.

92 (Tokyo, Japan). Adenine-induced CKD model mice were prepared as previously

93 described (44).

94 *CTX-induced muscle injury model*

95   A 50 µl volume of 10 µM CTX or an equal volume of phosphate buffered

96 saline (PBS) was injected into the gastrocnemius (GA) muscles using an insulin syringe

97 as described previously (45). On day 0, 3, 7, and 14 after CTX injection, the mice were

98 euthanized by intraperitoneally injecting an overdose of pentobarbital, and GA muscles

99 were removed and stored at −80°C until further use.

100 *Cell culture*

101   We used C2C12 myoblast cells to investigate the effect of excess iron on

102   skeletal muscle differentiation as described previously (29). The cells were grown to

103   sub-confluence for approximately 24–48 h, and incubated with either vehicle or iron

104   sulphate ($FeSO_4$) for 24 h. The culture medium was replaced with a differentiation

105   medium (DMEM) containing 2% horse serum, and incubated for the indicated

106   durations. In some experiments, the cells were pre-treated with 100 μM tempol and 50

107   μM DFO for 1 h before stimulation with iron. The treatment protocol of $FeSO_4$ and

108   tempol was determined in our previous study (29). We performed 3 to 6 well replicates

109   per experiment and repeated each experiment at least 2 times. C2C12 myoblast cells

110   were used until the 5th to 7th passages.

111   *RNA extraction and evaluation of mRNA expression levels*

112   The methods of RNA extraction, cDNA synthesis, and quantitative RT-PCR

113   have been previously described (46). In brief, the tissues were homogenized with the

114   Minilys beads-based homogenizer (Bertin Instruments, Montigny-le-Bretonneux,

115   France) in RNAiso reagent (Takara Bio, Otsu, Japan). RNA extraction and cDNA

116   synthesis were performed according to the manufacturer's instructions (PrimeScript RT

117   reagent kit with gDNA Eraser (Perfect Real Time), Takara Bio). Quantitative RT-PCR

118   was performed using the CFX Connect Real-Time PCR Detection System (Bio-Rad

119   Laboratories, Hercules, CA, USA) with THUNDERBIRD® SYBR® qPCR Mix

120   (TOYOBO Co., Ltd., Osaka, Japan). The primer sets used were: 5′-

121   GACTCCGGATGTGGAGAAAA-3′ and 5′-GAGCACTCGGCTAATCGAAC -3

122　′　　for *Pax-7*, 5 ′ - AGTGAATGAGGCTTCGAGA-3 ′ 　　and 5 ′

123　-CAGGATCTCCACCTTGGGTA-3 ′ 　　　　for *MyoD*, 5 ′ -

124　AGACGCCTGAAGAAGGTGAC-3′ and 5′-ACCTTGGGGAGTCTCTTCAA-3′

125　for *Myf5*, 5 ′ - CACGATGGACGTAAGGGAGT -3 ′ 　and 5 ′ -

126　CCAGATGGACGTAAGGGAGT-3 ′ 　　for *Myogenin*, 5 ′ -

127　AGAGTCTGTCAAGGCCCTGA-3′ and 5′ - CAGCCTGCCTCTTGTAGGAC-3′

128　for *Myh3* (*embryonic Myh*), 5′-GAGCGGAGAGTACTGGATCG-3′ and 5′

129　-GTTCGGGCTGATGTACCAGT-3′ for *collagen type I alpha 1 chain* (*Col1a1*), 5′

130　-GTGTTCAAGGTGGCAAAGGT-3′ and 5′-GACCGAATTCACCAGGAAGA-3

131　′　　for *collagen type I alpha 2 chain* (*Col1a2*), 5 ′

132　-ACCAAAAGGTGATGCTGGAC-3′ and 5′-GACCTCGTGCTCCAGTTAGC-3

133　′　　for *collagen type III alpha 1 chain* (*Col3a1*), 5 ′

134　-TGAGTGGCTGTCTTTTGACG-3′ and 5′-AGCCCTGTATTCCGTCTCCT-3′

135　for *transforming growth factor-beta 1* (*Tgf-β1*), 5 ′

136　-CTGTAACCGGATGGCAAACT-3′ and 5′-CTGTACCCACATGGCTGATG-3′

137　for *F4/80*, and 5 ′ -GCTCCAAGCAGATGCAGCA-3 ′ 　　and 5 ′

138　-CCGGATGTGAGGCAGCAG-3′ for *36B4* (internal control). The expression levels

139　of all target genes were normalized using *36B4* expression, and the values were

140　compared to the control group in terms of relative fold changes.

141　*Protein extraction and western blot analysis*

142   Protein extraction and western blotting were performed as previously

143   described (46). The tissue or cell samples were homogenized or sonicated in a protein

144   lysis buffer containing inhibitors of proteinase and phosphatase, and the proteins were

145   extracted. The extracted proteins were boiled for 5 min in Laemmli sample buffer and

146   used for western blotting. The detected immune-reactive bands were quantified by

147   densitometric analysis using Image J (version 1.38) software (National Institutes of

148   Health, Bethesda, MD, USA) as described previously (47). Phosphorylation specific

149   signals are normalized against levels of total target protein, and protein expression is

150   normalized using tubulin as an internal loading control.

151   *Histological analysis*

152   GA muscles were fixed overnight in 4% paraformaldehyde at 4°C and

153   embedded in paraffin. Sections 3 μm in thickness were prepared and stained with

154   hematoxylin-eosin to measure the area of muscle fiber. Area measurements of at least

155   100 fibers were obtained for each animal from 10 randomly selected fields in five

156   different sections. Muscle fiber area was quantified using Image J (version 1.38)

157   software. The regenerating myofibers were indicated as myofibers with centralized

158   nuclei. Picrosirius red staining was used for evaluating skeletal muscle fibrosis as

159   previously described (48).

160   *Fusion index*

9

161   Forty-eight hours after the initiation of muscle differentiation, C2C12 cells

162   were fixed with 4% paraformaldehyde for 10 min and stained with anti-Myh3 overnight

163   at 4°C and mounted using mounting medium 4′,6-diamidino-2-phenylindole (DAPI,

164   VECTASHIELD; Vector Laboratories, Burlingame, CA, USA). Five different fields per

165   well were randomly selected and the number of nuclei in each myotube and the total

166   number of nuclei in cells were counted in each field. The fusion index was calculated as

167   the percentage of the total number of nuclei in Myh-positive cells from the total number

168   of nuclei counted in the field.

169   *In situ superoxide detection*

170   Superoxide production in the skeletal muscle was detected by the

171   dihydroethidium (DHE) staining method as described previously (29). Non-fixed frozen

172   tissue sections were incubated with DHE in PBS (10 μM) in a dark, humidified

173   container at room temperature for 30 min and then observed using a fluorescence

174   microscope.

175   In situ *detection of labile ferrous iron and hydroxyl radicals*

176   Labile ferrous iron and hydroxyl radicals were detected by RhoNox-1 (49)

177   and HPF, respectively. In brief, the frozen sections were fixed in 10% neutral

178   formaldehyde for 1 min, washed with HBSS, and incubated with 5 μM RhoNox-1 and 5

179   μM HPF in a dark, humidified container at room temperature for 30 min. After washing,

180 the section was observed using fluorescence microscopy (46). RhoNox-1 was

181 synthesized according to the literature procedure (49).

182 *TBARS assay*

183   A thiobarbituric acid reactive substance (TBARS) assay was used to measure

184 malondialdehyde (MDA) concentration in skeletal muscles as previously described

185 (13). The suspension of homogenized muscle tissue that was not centrifuged was used

186 for the assay.

187 *Measurement of oxidative stress in C2C12 myoblast cells*

188   Intracellular reactive oxidative species were detected and quantified using $2'$

189 $, 7'$ -dichlorofluorescin diacetate (DCFH-DA; Sigma-Aldrich) as described previously

190 (46).

191 *Cell viability assay*

192   Cell proliferation was accessed using a CellTiter 96 AQueous non-radioactive

193 cell proliferation assay kit (Promega KK, Tokyo, Japan) (46). Cytotoxicity was

194 evaluated using a Cytotoxicity LDH Assay Kit-WST (DOJINDO LABORATORIES,

195 Kumamoto, Japan) according to the manufacturer's instructions. Briefly, C2C12

196 myoblast cells were seeded in 96-well plates at a cell concentration of 1×10^4 cells per

197 well and incubated for 24 h. When the cell growth was sub-confluent, $FeSO_4$ was added

198 and the cells were cultured in DMEM with or without fetal bovine serum (FBS) for 24

199 h. The proliferation or cytotoxicity of cells was assessed with MTS assay or LDH assay

200 by measuring the absorbance at 490 nm using an iMARK microplate reader (Bio-Rad

201 Laboratories).

202 *Quantification of iron content*

203 Iron content of tissues or cells was measured using an iron assay kit according

204 to the manufacturer's instructions (Metallo assay LS, Metallogenics, Chiba, Japan) as

205 described previously (29). Iron concentration was evaluated using tissue-weight or

206 protein concentration and expressed as µg Fe per g of wet tissue or µg Fe per protein

207 concentration.

208 *Measurement of p38MAPK activity*

209 The activity of p38MAPK was measured using a commercially available kit

210 according to the manufacturer's instructions (CycLex p38 Kinase Assay/Inhibitor

211 Screening Kit, MEDICAL and BIOLOGICAL LABORATORIES Co., Ltd., Nagoya,

212 Japan).

213 *Statistical analysis*

214 Data are presented as mean ± standard deviation (mean ± SD). Mann–Whitney

215 U test was used for comparisons between the two groups. For comparisons between

216 more than two groups, the statistical significance of each difference was evaluated using

217 the Kruskal–Wallis test. Statistical significance was indicated by $P < 0.05$.

218 **Results**

219 *Iron content of skeletal muscle in mouse models of aging, diabetes, and CKD*

220   Skeletal muscle regeneration is suppressed during muscle wasting due to

221   aging in humans (41), in addition to diabetes (37) and CKD (40) in mice. We first

222   evaluated iron accumulation in skeletal muscle under the above conditions using a

223   mouse model involving aged mice (2-years-of-age), *db/db* mice (type 2 diabetic model),

224   and CKD mice (adenine-induction), respectively. Iron content (Figure 1A), as well as

225   FTH and FTL protein expression (Supplementary figure), were elevated in skeletal

226   muscle with aging, diabetes, and CKD. Similar to iron content, oxidative stress was also

227   increased in skeletal muscles with aging, diabetes, and CKD (Figure 1B). In terms of

228   mRNA expression of satellite cell markers, *Pax-7*, *MyoD*, and *Myf5* were significantly

229   reduced in skeletal muscles of mice with diabetes and CKD. Aged mice displayed

230   reduced mRNA expression of *Pax-7* and *Myf5*, but not *MyoD*, in skeletal muscles

231   (Figure 1C). Iron accumulation in skeletal muscle might cause the decline of satellite

232   cells by increasing oxidative stress. Therefore, iron is a potential problem for impaired

233   myogenesis in aging, diabetes, and CKD.

234   *Effect of iron overload on skeletal muscle*

235   To evaluate the effect of excess iron on muscle regeneration, we used mice

236   with iron overload. The iron overload model showed that there were no differences in

237   body weight and skeletal muscle weight between vehicle- and iron-treated mice (Table.

238   1). Iron content as well as the protein expression of FTH and FTL were increased in

239   mice with iron overload (Figures 2A and B). Oxidative stress markers, such as DHE

240   intensity and TBARS concentration, were increased in skeletal muscles of mice with

241   iron overload (Figures 2C and D). The mRNA expression of satellite cell markers *Pax-7*

242   and *MyoD* was significantly reduced in skeletal muscles of mice with iron overload

243   (Figure 2E). Similarly, the number of Pax-7 positive cells was reduced in skeletal

244   muscles of iron-treated mice (Figure 2F). However, there were no differences in muscle

245   fiber area as well as mRNA expression of atrogin-1 and MuRF1 between

246   vehicle-treated mice and iron-treated mice (Figure 2G and H).

247   *Suppressive action of iron accumulation on skeletal muscle regeneration after*

248   *CTX-induced injury*

249   To examine the effect of iron accumulation on skeletal muscle regeneration, CTX was

250   injected in the skeletal muscles of mice. The mRNA expression of myogenic

251   transcription factors *myogenin* and *Myh3* were upregulated in muscles after CTX injury.

252   However, their mRNA expression was downregulated in mice with iron overload

253   (Figure 3A). Histological analysis revealed that mice with iron overload showed

254   reduced number of regenerated muscle fibers with centralized nuclei as well as muscle

255   fiber area after CTX injury on day 7 and day 15 compared to control mice (Figures 3B

256   and C). In addition, fibrosis-related genes (*Col1a1*, *Col1a2*, *Col3a1*, and *Tgf-β1*

257   mRNA) were highly expressed in muscle of the iron-treated group at day3 or 7 and later

258   after CTX injury (Figure 3D). Collagen deposition was increased in CTX-injured

259   muscle at day 15 of iron overload as visualized in histology with picrosirius red staining.

260   On the contrary, no differences in the expression of the macrophage marker F4/80 were

261   observed in skeletal muscle between the vehicle- and iron-treated groups (data not

14

262 shown). The p38MAPK-dependent pathway plays a pivotal role in the activation of

263 myogenic differentiation (50). Diabetic and CKD mice, not aged mice, showed the

264 reduced phosphorylation of p38MAPK and ERK1/2 (Figure 1D and E).

265 Phosphorylation of p38MAPK was upregulated in skeletal muscles after CTX injury on

266 day 3, day 7 and day 14, which was suppressed by iron overload. Similar to p38MAPK,

267 the degree of ERK1/2 phosphorylation was also lower on day 3 and 7 in CTX-injured

268 muscle of mice with iron overload (Figure 3F).

269 *Inhibitory action of iron on C2C12 myoblast differentiation*

270 To examine the mechanism of inhibitory effect of iron on skeletal muscle

271 regeneration, we used C2C12 myoblast cells. The proliferative activity of these cells

272 was prevented by iron treatment in the presence or absence of serum in the culture

273 media. We also tested cytotoxicity of iron by LDH assay, and iron treatment increased

274 LDH release independent of the presence or absence of serum in the culture media

275 (Figure 4A). C2C12 myoblast cells were differentiated with an increase in *Myh* and

276 *myogenin* mRNA expression after transfer of cells to differentiation media, which

277 inhibited by concomitant treatment with iron (Figures 4B). The fusion index of

278 myotubes was also reduced by iron treatment (Figure 4C). p38MAPK phosphorylation

279 was significantly higher in C2C12 myoblast cells treated with iron before differentiation.

280 However, the increase in p38MAPK phosphorylation was even lower 5 and 10 min after

281 transfer to the differentiation media in iron-loaded C2C12 myoblast cells compared with

282 vehicle-loaded cells. ERK1/2 phosphorylation was also higher in C2C12 myoblast cells

15

283 at 10, 15, and 30 min after transfer to the differentiation media, which was suppressed

284 in iron-loaded culture media beforehand (Figure 4D). Similar to p38MAPK

285 phosphorylation, p38MAPK activity was increased after the changing to differentiation

286 media. This increase was lowered by iron treatment (Figure 5F).

287 *Involvement of oxidative stress in iron-mediated suppression of C2C12 myoblast*

288 *differentiation*

289 In C2C12 myoblast cells, oxidative stress was induced by iron overload,

290 which was later suppressed by the superoxide scavenger tempol (Figure 5B). The iron

291 content was also increased by iron treatment. However, tempol did not change the

292 increased iron content (Figure 5A). Iron-induced inhibition of C2C12 myoblast

293 differentiation, which lead to a reduction in mRNA expression of *myogenin* and *Myh* as

294 well as decrease in fusion index, was restored by tempol pre-treatment (Figures 5C and

295 D). Tempol partially ameliorated the reduced phosphorylation of p38MAPK and

296 ERK1/2, which was inhibited by iron treatment 5 min or more after transfer to the

297 differentiation medium (Figure 5E). In addition, tempol reversed the reduced

298 p38MAPK activity with iron treatment 5 min after the change to differentiation medium

299 (Figure 5G). In addition, DFO, an iron chelator, partly ameliorated iron-mediated

300 inhibition of myoblast differentiation (Supplementary figure 2).

301 **Discussion**

16

302   Iron accumulation has a harmful effect on myogenesis due to oxidative stress,

303   causing imbalance in skeletal muscle homeostasis. Presently, the suppression of skeletal

304   muscle regeneration due to iron overload, the increment of oxidative stress in a mouse

305   model of CTX injury, and the inhibitory action of iron on muscle differentiation were

306   all recovered by tempol *in vitro*.

307   Skeletal muscle mass is determined and regulated by the coordinated balance

308   between muscle degradation and regeneration. Disruption of this balance leads to a

309   decrease in skeletal muscle mass, which is known as sarcopenia. Excess iron causes

310   skeletal muscle atrophy by inducing protein degradation due to oxidative stress (28, 29).

311   In the present study, excess iron also impaired myogenesis due to oxidative stress. Our

312   findings suggested that iron plays a pivotal role in the loss of skeletal muscle mass

313   through its anti-myogenesis properties.

314   Mice with excess iron showed reduced mRNA expression of the satellite cell

315   markers *Pax-7* and *MyoD* in skeletal muscle under basal conditions. The activation of

316   satellite cell markers is an important event during muscle repair and regeneration in

317   mice (51, 52). Conversely, inactivation of these markers occurs with age or disease. The

318   number and function of satellite cell markers are also reduced and impaired in muscles

319   of mice with advancing age (35, 36, 53). The expression of *Pax-7* and *MyoD* is

320   decreased in skeletal muscles of mice with CKD (40) and diabetes (37-39). In humans,

321   satellite cell numbers and Pax-7 expression decrease in skeletal muscle with aging

322   relative to those during youth (41, 42), and myogenic potential of satellite cells is

17

323 compromised in aging human muscle (54). Moreover, there is a decline in the capacity

324 of muscle regeneration with increasing age in both mice and humans (55-57),

325 suggesting skeletal muscle loss mediated by the reduction of myogenesis. We found

326 that iron concentration was elevated and that satellite cell markers were reduced in

327 skeletal muscles in mouse models of aging, CKD, and diabetes. Oxidative stress

328 influences both the function and proliferation of satellite cells (58). Oxidative stress was

329 increased in the skeletal muscle of the mouse models. Therefore, iron accumulation

330 might augment oxidative stress and promote the decline of both satellite cell number

331 and function, resulting in impaired muscle regeneration. Satellite cells are generally

332 thought to be essential during muscle regeneration. A recent study has shown that

333 expression of Pax-7 in satellite cells is lower, and the exercise-induced satellite cell

334 response is blunted in skeletal muscle of old mice (32). On the other hand, satellite cell

335 numbers do not decline in human muscle with aging (59), and there is no difference in

336 the proliferative response of satellite cells between children and adults (58). There is no

337 difference in satellite cell numbers between young and aged mice although an

338 age-related decline in myoblast generation is seen in response to injury (60). Thus,

339 studies of age-related decreases in satellite cell number and function have to date

340 yielded contradictory results. Therefore, further studies are necessary for clarifying the

341 role of satellite cells in impaired muscle regeneration and muscle loss during aging

342 conditions, as well as in disease states such as diabetes and CKD.

343   CTX-injured muscle showed increased *Tgf-β1*, *Col1* and *Col3* mRNA and

344   collagen deposition, and these were higher in mice with iron overload, resulting in the

345   promotion of excessive fibrosis. Similar to skeletal muscle, iron causes tissue fibrosis in

346   cardiovascular organs (15, 61), kidney (14, 62), and liver (63) in mouse disease models.

347   The interaction between fibroblasts and satellite cells is important in the regulation of

348   myogenesis (64). Abnormal extracellular matrix deposition and fibrosis are known to

349   impair muscle regeneration after acute injury (65, 66). Deletion of satellite cells also

350   enhances muscle fibrosis after CTX-injury (64). Therefore, increased fibrosis, as well as

351   reduced satellite cell numbers, might lead to compromised myogenesis after CTX injury

352   under iron overload.

353   CTX-injured muscle regeneration has been widely accepted as a valid means

354   of investigating the mechanism of skeletal muscle regeneration and differentiation (67).

355   Generally, the expression of *myogenin* and *Myh* are upregulated and regenerative

356   muscle fibers with centered nuclei are seen during muscle regeneration after CTX injury

357   (40, 68). In the present study, iron-treated mice displayed suppressed upregulation of

358   *myogenin* and *Myh3* mRNA expression and the regenerative muscle fibers with central

359   nuclei were reduced in injured muscle with CTX compared to vehicle-treated mice. This

360   indicates the involvement of iron in impaired muscle regeneration. In addition, the

361   phosphorylated levels of p38MAPK and ERK1/2 were increased in CTX-injured

362   muscle. However, the increase in phosphorylated levels was also lowered in skeletal

363   muscles of mice treated with excess iron. The p38MAPK signaling pathway is crucial in

19

364 regulating skeletal muscle gene expression at different stages of the myogenic process

365 (69). p38MAPK promotes skeletal muscle differentiation via activation of the MEF2C

366 transcription factor (50, 70). Thus, p38MAPK activation is essential for skeletal muscle

367 differentiation and regeneration. In the light of ERK1/2 action on skeletal muscle

368 differentiation, ERK1/2 activation also seems to promote skeletal muscle differentiation

369 in a similar manner along with the p38MAPK signaling pathway. Inhibition of ERK1/2

370 signaling suppresses multinucleated myotube formation and decreases the expression of

371 muscle-specific genes (*MyoD* and *myogenin*) in myoblasts after the induction of

372 differentiation (70-72). However, ERK1/2 is reportedly required for myoblast

373 proliferation, but not for differentiation (73, 74). Thus, the role of the ERK1/2 pathway

374 on skeletal muscle differentiation is still controversial and further research is needed to

375 clarify this aspect.

376   In the present study, excess iron increased ferrous iron and reactive oxygen

377 species (ROS) abundance in skeletal muscle, suggesting the occurrence of the Fenton

378 reaction under iron overload. C2C12 myoblast differentiation was impaired under iron

379 overload conditions, and the free radical scavenger tempol ameliorated iron-mediated

380 reduction of myoblast differentiation and MAPK activity, indicating the involvement of

381 excess iron-mediated oxidative stress in impaired muscle differentiation via inactivation

382 of the p38MAPK and ERK1/2 signaling pathways. We have previously shown that iron

383 reduces Akt-FOXO3a phosphorylation and that this phosphorylation is prevented by

384 tempol (29). Therefore, iron-mediated oxidative stress might be involved in the

385 suppression of the aforementioned kinase pathway. Previous studies have shown that

386 oxidative stress induced by hydrogen peroxide or creatinine directly impairs muscle

387 differentiation in C2C12 myoblast cells (75-77). Tumor necrosis factor-alpha-induced

388 oxidative stress is involved in impaired muscle differentiation in tumor-bearing mice

389 (78). Thus, ROS can generally cause inhibition of myogenic differentiation (75, 76, 79),

390 and this action cannot be attributed solely to increased cell death (77). ROS can increase

391 nuclear factor-kappa B (NF-κB) activity (75), which inhibits skeletal muscle

392 differentiation (80, 81). Taken together, iron overload might promote ROS-mediated

393 impaired myogenesis.

394 On the other hand, oxidative stress also plays an important signaling role in

395 skeletal muscle adaptation (82). Contrary to our findings, oxidative stress induced by

396 hydrogen peroxide activates the p38MAPK and ERK1/2 pathways through NF-κB

397 transactivation in skeletal myoblasts (83). Therefore, the effect of oxidative stress on

398 myogenesis has dual physiological and pathological aspects and is controversial (84).

399 More research is necessary to further elucidate the inhibitory mechanisms of iron on

400 myogenesis.

401 Iron deficiency is an acknowledged concern, and functional foods amended

402 with iron are commercially available to prevent iron deficiency. However, as previously

403 mentioned, the iron content in the human body increases with age and in diseases,

404 including diabetes and CKD, indicating increased iron content in skeletal muscle. The

405 level of iron intake is important. Excess iron intake impairs regeneration of skeletal

21

406 muscle and can induce muscle atrophy. Muscle atrophy and degradation in the presence

407 of excess iron also involves the oxidative stress-ubiquitin ligase E3 pathway (29). Thus,

408 iron deficiency and excess can be detrimental.

409   In conclusion, iron overload affects skeletal muscle differentiation, possibly

410 through oxidative stress-dependent inhibition of the p38 MAPK and ERK1/2 signaling

411 pathways. This finding suggests a crucial role of iron in muscle regeneration, and

412 clarifies the underlying mechanisms of skeletal muscle homeostasis.

413

420

421 **Conflict of Interest Statement**

422 The authors declare no conflict of interests.

423

424 **Author Contributions**

References

1. Camaschella, C. (2005) Understanding iron homeostasis through genetic analysis of hemochromatosis and related disorders. *Blood* **106**, 3710-3717

2. Hayashi, H., Takikawa, T., Nishimura, N., and Yano, M. (1995) Serum aminotransferase levels as an indicator of the effectiveness of venesection for chronic hepatitis C. *J Hepatol* **22**, 268-271

3. Iwasaki, T., Nakajima, A., Yoneda, M., Yamada, Y., Mukasa, K., Fujita, K., Fujisawa, N., Wada, K., and Terauchi, Y. (2005) Serum ferritin is associated with visceral fat area and subcutaneous fat area. *Diabetes Care* **28**, 2486-2491

4. Ford, E. S., and Cogswell, M. E. (1999) Diabetes and serum ferritin concentration among U.S. adults. *Diabetes Care* **22**, 1978-1983

5. Lee, D. H., Liu, D. Y., Jacobs, D. R., Jr., Shin, H. R., Song, K., Lee, I. K., Kim, B., and Hider, R. C. (2006) Common presence of non-transferrin-bound iron among patients with type 2 diabetes. *Diabetes Care* **29**, 1090-1095

6. Salonen, J. T., Nyyssonen, K., Korpela, H., Tuomilehto, J., Seppanen, R., and Salonen, R. (1992) High stored iron levels are associated with excess risk of myocardial infarction in eastern Finnish men. *Circulation* **86**, 803-811

7. Menke, A., Fernandez-Real, J. M., Muntner, P., and Guallar, E. (2009) The association of biomarkers of iron status with peripheral arterial disease in US adults. *BMC Cardiovasc Disord* **9**, 34

8. Nakanishi, T., Kuragano, T., Nanami, M., Otaki, Y., Nonoguchi, H., and Hasuike, Y. (2010) Importance of ferritin for optimizing anemia therapy in chronic kidney disease. *American journal of nephrology* **32**, 439-446

9. Hayashi, H., Takikawa, T., Nishimura, N., Yano, M., Isomura, T., and Sakamoto, N. (1994) Improvement of serum aminotransferase levels after phlebotomy in patients with chronic active hepatitis C and excess hepatic iron. *Am J Gastroenterol* **89**, 986-988

10. Fernandez, E., Blanco, C., Garcia, S., Dieguez, A., Riestra, S., and Rodrigo, L. (2005) Use of low concentrations of human IgA anti-tissue transglutaminase to rule out selective IgA deficiency in patients with suspected celiac disease. *Clin Chem* **51**, 1014-1016

11. Houschyar, K. S., Ludtke, R., Dobos, G. J., Kalus, U., Broecker-Preuss, M., Rampp, T., Brinkhaus, B., and Michalsen, A. (2012) Effects of phlebotomy-induced reduction of body iron stores on metabolic syndrome: results from a randomized clinical trial. *BMC Med* **10**, 54

12. Tajima, S., Ikeda, Y., Sawada, K., Yamano, N., Horinouchi, Y., Kihira, Y., Ishizawa, K., Izawa-Ishizawa, Y., Kawazoe, K., Tomita, S., Minakuchi, K., Tsuchiya, K., and Tamaki, T. (2012) Iron reduction by deferoxamine leads to amelioration of adiposity via the regulation of oxidative stress and inflammation in obese and type 2 diabetes KKAy mice. *Am J Physiol Endocrinol Metab* **302**, E77-86

13. Ikeda, Y., Enomoto, H., Tajima, S., Izawa-Ishizawa, Y., Kihira, Y., Ishizawa, K., Tomita, S., Tsuchiya, K., and Tamaki, T. (2013) Dietary iron restriction inhibits progression of diabetic nephropathy in db/db mice. *American journal of physiology. Renal physiology* **304**, F1028-1036

14. Ikeda, Y., Horinouchi, Y., Hamano, H., Hirayama, T., Kishi, S., Izawa-Ishizawa, Y., Imanishi, M., Zamami, Y., Takechi, K., Miyamoto, L., Ishizawa, K., Aihara, K. I., Nagasawa, H., Tsuchiya, K., and Tamaki, T. (2017) Dietary iron restriction alleviates renal tubulointerstitial injury induced by protein overload in mice. *Sci Rep* **7**, 10621

15. Naito, Y., Hirotani, S., Sawada, H., Akahori, H., Tsujino, T., and Masuyama, T. (2011) Dietary iron restriction prevents hypertensive cardiovascular remodeling in dahl salt-sensitive rats. *Hypertension* **57**, 497-504

16. Sawada, H., Hao, H., Naito, Y., Oboshi, M., Hirotani, S., Mitsuno, M., Miyamoto, Y., Hirota, S., and Masuyama, T. (2015) Aortic iron overload with oxidative stress and inflammation in human and murine abdominal aortic aneurysm. *Arterioscler Thromb Vasc Biol* **35**, 1507-1514

17. Evans, W. J. (1995) What is sarcopenia? *The journals of gerontology. Series A, Biological sciences and medical sciences* **50 Spec No**, 5-8

18. Fulster, S., Tacke, M., Sandek, A., Ebner, N., Tschope, C., Doehner, W., Anker, S. D., and von Haehling, S. (2013) Muscle wasting in patients with chronic heart failure: results from the studies investigating co-morbidities aggravating heart failure (SICA-HF). *European heart journal* **34**, 512-519

19. Mak, R. H., Ikizler, A. T., Kovesdy, C. P., Raj, D. S., Stenvinkel, P., and Kalantar-Zadeh, K. (2011) Wasting in chronic kidney disease. *Journal of cachexia, sarcopenia and muscle* **2**, 9-25

20. Kim, T. N., Park, M. S., Yang, S. J., Yoo, H. J., Kang, H. J., Song, W., Seo, J. A., Kim, S. G., Kim, N. H., Baik, S. H., Choi, D. S., and Choi, K. M. (2010) Prevalence and determinant factors of sarcopenia in patients with type 2 diabetes: the Korean Sarcopenic Obesity Study (KSOS). *Diabetes Care* **33**, 1497-1499

21. Lim, S., Kim, J. H., Yoon, J. W., Kang, S. M., Choi, S. H., Park, Y. J., Kim, K. W., Lim, J. Y., Park, K. S., and Jang, H. C. (2010) Sarcopenic obesity: prevalence and association with metabolic syndrome in the Korean Longitudinal Study on Health and Aging (KLoSHA). *Diabetes Care* **33**, 1652-1654

22. Lynch, G. S. (2001) Therapies for improving muscle function in neuromuscular disorders. *Exercise and sport sciences reviews* **29**, 141-148

23. Kim, T. H., Hwang, H. J., and Kim, S. H. (2014) Relationship between serum ferritin levels and sarcopenia in Korean females aged 60 years and older using the fourth Korea National Health and Nutrition Examination Survey (KNHANES IV-2, 3), 2008-2009. *PloS one* **9**, e90105

24. Chung, J. Y., Kang, H. T., Lee, D. C., Lee, H. R., and Lee, Y. J. (2013) Body composition and its association with cardiometabolic risk factors in the elderly: a focus on sarcopenic obesity. *Archives of gerontology and geriatrics* **56**, 270-278

25. Altun, M., Edstrom, E., Spooner, E., Flores-Moralez, A., Bergman, E., Tollet-Egnell, P., Norstedt, G., Kessler, B. M., and Ulfhake, B. (2007) Iron load and redox stress in skeletal muscle of aged rats. *Muscle & nerve* **36**, 223-233

26. DeRuisseau, K. C., Park, Y. M., DeRuisseau, L. R., Cowley, P. M., Fazen, C. H., and Doyle, R. P. (2013) Aging-related changes in the iron status of skeletal muscle. *Experimental gerontology* **48**, 1294-1302

27. Xu, J., Knutson, M. D., Carter, C. S., and Leeuwenburgh, C. (2008) Iron accumulation with age, oxidative stress and functional decline. *PloS one* **3**, e2865

28. Reardon, T. F., and Allen, D. G. (2009) Iron injections in mice increase skeletal muscle iron content, induce oxidative stress and reduce exercise performance. *Experimental physiology* **94**, 720-730

29. Ikeda, Y., Imao, M., Satoh, A., Watanabe, H., Hamano, H., Horinouchi, Y., Izawa-Ishizawa, Y., Kihira, Y., Miyamoto, L., Ishizawa, K., Tsuchiya, K., and Tamaki, T. (2016) Iron-induced skeletal muscle atrophy involves an Akt-forkhead box O3-E3 ubiquitin ligase-dependent pathway. *Journal of trace elements in medicine and biology : organ of the Society for Minerals and Trace Elements* **35**, 66-76

30. Phillips, S. M., Glover, E. I., and Rennie, M. J. (2009) Alterations of protein turnover underlying disuse atrophy in human skeletal muscle. *J Appl Physiol (1985)* **107**, 645-654

31. Seale, P., Sabourin, L. A., Girgis-Gabardo, A., Mansouri, A., Gruss, P., and Rudnicki, M. A. (2000) Pax7 is required for the specification of myogenic satellite cells. *Cell* **102**, 777-786

32. Moore, D. R., McKay, B. R., Tarnopolsky, M. A., and Parise, G. (2018) Blunted satellite cell response is associated with dysregulated IGF-1 expression after exercise with age. *Eur J Appl Physiol* **118**, 2225-2231

33. Cornelison, D. D., and Wold, B. J. (1997) Single-cell analysis of regulatory gene expression in quiescent and activated mouse skeletal muscle satellite cells. *Dev Biol* **191**, 270-283

34. Olguin, H. C., Yang, Z., Tapscott, S. J., and Olwin, B. B. (2007) Reciprocal inhibition between Pax7 and muscle regulatory factors modulates myogenic cell fate determination. *J Cell Biol* **177**, 769-779

35. Gibson, M. C., and Schultz, E. (1983) Age-related differences in absolute numbers of skeletal muscle satellite cells. *Muscle & nerve* **6**, 574-580

36. Brack, A. S., Conboy, M. J., Roy, S., Lee, M., Kuo, C. J., Keller, C., and Rando, T. A. (2007) Increased Wnt signaling during aging alters muscle stem cell fate and increases fibrosis. *Science* **317**, 807-810

37. Fu, X., Zhu, M., Zhang, S., Foretz, M., Viollet, B., and Du, M. (2016) Obesity Impairs Skeletal Muscle Regeneration Through Inhibition of AMPK. *Diabetes* **65**, 188-200

38. D'Souza, D. M., Zhou, S., Rebalka, I. A., MacDonald, B., Moradi, J., Krause, M. P., Al-Sajee, D., Punthakee, Z., Tarnopolsky, M. A., and Hawke, T. J. (2016) Decreased Satellite Cell Number and Function in Humans and Mice With Type 1 Diabetes Is the Result of Altered Notch Signaling. *Diabetes* **65**, 3053-3061

39. Fujimaki, S., Wakabayashi, T., Asashima, M., Takemasa, T., and Kuwabara, T. (2016) Treadmill running induces satellite cell activation in diabetic mice. *Biochem Biophys Rep* **8**, 6-13

40. Zhang, L., Wang, X. H., Wang, H., Du, J., and Mitch, W. E. (2010) Satellite cell dysfunction and impaired IGF-1 signaling cause CKD-induced muscle atrophy. *J Am Soc Nephrol* **21**, 419-427

41. Renault, V., Thornell, L. E., Eriksson, P. O., Butler-Browne, G., and Mouly, V. (2002) Regenerative potential of human skeletal muscle during aging. *Aging Cell* **1**, 132-139

42. Verdijk, L. B., Koopman, R., Schaart, G., Meijer, K., Savelberg, H. H., and van Loon, L. J. (2007) Satellite cell content is specifically reduced in type II skeletal muscle fibers in the elderly. *Am J Physiol Endocrinol Metab* **292**, E151-157

43. Kuo, K. L., Hung, S. C., Lee, T. S., and Tarng, D. C. (2014) Iron sucrose accelerates early atherogenesis by increasing superoxide production and upregulating adhesion molecules in CKD. *J Am Soc Nephrol* **25**, 2596-2606

44. Hamano, H., Ikeda, Y., Watanabe, H., Horinouchi, Y., Izawa-Ishizawa, Y., Imanishi, M., Zamami, Y., Takechi, K., Miyamoto, L., Ishizawa, K., Tsuchiya, K., and Tamaki, T. (2018) The uremic toxin indoxyl sulfate interferes with iron metabolism by regulating hepcidin in chronic kidney disease. *Nephrol Dial Transplant* **33**, 586-597

45. Zeng, L., Akasaki, Y., Sato, K., Ouchi, N., Izumiya, Y., and Walsh, K. (2010) Insulin-like 6 is induced by muscle injury and functions as a regenerative factor. *J Biol Chem* **285**, 36060-36069

46. Oshima, K., Ikeda, Y., Horinouchi, Y., Watanabe, H., Hamano, H., Kihira, Y., Kishi, S., Izawa-Ishizawa, Y., Miyamoto, L., Hirayama, T., Nagasawa, H., Ishizawa, K., Tsuchiya, K., and Tamaki, T. (2017) Iron suppresses erythropoietin expression via oxidative stress-dependent hypoxia-inducible factor-2 alpha inactivation. *Laboratory investigation; a journal of technical methods and pathology* **97**, 555-566

47. Gassmann, M., Grenacher, B., Rohde, B., and Vogel, J. (2009) Quantifying Western blots: pitfalls of densitometry. *Electrophoresis* **30**, 1845-1855

48. Horinouchi, Y., Ikeda, Y., Fukushima, K., Imanishi, M., Hamano, H., Izawa-Ishizawa, Y., Zamami, Y., Takechi, K., Miyamoto, L., Fujino, H., Ishizawa, K., Tsuchiya, K., and Tamaki, T. (2018) Renoprotective effects of a factor Xa inhibitor: fusion of basic research and a database analysis. *Sci Rep* **8**, 10858

49. Hirayama, T., Okuda, T., and Nagasawa, H. (2013) A highly selective turn-on fluorescent probe fro iron(II) to visualize labile iron in living cells. *Chem Sci* **4**, 1250-1256

50. Zetser, A., Gredinger, E., and Bengal, E. (1999) p38 mitogen-activated protein kinase pathway promotes skeletal muscle differentiation. Participation of the Mef2c transcription factor. *J Biol Chem* **274**, 5193-5200

51. Lepper, C., Partridge, T. A., and Fan, C. M. (2011) An absolute requirement for Pax7-positive satellite cells in acute injury-induced skeletal muscle regeneration. *Development* **138**, 3639-3646

52. Cooper, R. N., Tajbakhsh, S., Mouly, V., Cossu, G., Buckingham, M., and Butler-Browne, G. S. (1999) In vivo satellite cell activation via Myf5 and MyoD in regenerating mouse skeletal muscle. *J Cell Sci* **112 (Pt 17)**, 2895-2901

53. Gallegly, J. C., Turesky, N. A., Strotman, B. A., Gurley, C. M., Peterson, C. A., and Dupont-Versteegden, E. E. (2004) Satellite cell regulation of muscle mass is altered at old age. *J Appl Physiol (1985)* **97**, 1082-1090

54. Corbu, A., Scaramozza, A., Badiali-DeGiorgi, L., Tarantino, L., Papa, V., Rinaldi, R., D'Alessandro, R., Zavatta, M., Laus, M., Lattanzi, G., and Cenacchi, G. (2010) Satellite cell characterization from aging human muscle. *Neurol Res* **32**, 63-72

55. Cartee, G. D. (1995) What insights into age-related changes in skeletal muscle are provided by animal models? *The journals of gerontology. Series A, Biological sciences and medical sciences* **50 Spec No**, 137-141

56. Grounds, M. D. (1998) Age-associated changes in the response of skeletal muscle cells to exercise and regeneration. *Ann N Y Acad Sci* **854**, 78-91

57. Bross, R., Storer, T., and Bhasin, S. (1999) Aging and Muscle Loss. *Trends Endocrinol Metab* **10**, 194-198

58. Renault, V., Thornell, L. E., Butler-Browne, G., and Mouly, V. (2002) Human skeletal muscle satellite cells: aging, oxidative stress and the mitotic clock. *Experimental gerontology* **37**, 1229-1236

59. Roth, S. M., Martel, G. F., Ivey, F. M., Lemmer, J. T., Metter, E. J., Hurley, B. F., and Rogers, M. A. (2000) Skeletal muscle satellite cell populations in healthy young and older men and women. *Anat Rec* **260**, 351-358

60. Conboy, I. M., Conboy, M. J., Smythe, G. M., and Rando, T. A. (2003) Notch-mediated restoration of regenerative potential to aged muscle. *Science* **302**, 1575-1577

61. Ishizaka, N., Saito, K., Mitani, H., Yamazaki, I., Sata, M., Usui, S., Mori, I., Ohno, M., and Nagai, R. (2002) Iron overload augments angiotensin II-induced cardiac fibrosis and promotes neointima formation. *Circulation* **106**, 1840-1846

62. Ikeda, Y., Ozono, I., Tajima, S., Imao, M., Horinouchi, Y., Izawa-Ishizawa, Y., Kihira, Y., Miyamoto, L., Ishizawa, K., Tsuchiya, K., and Tamaki, T. (2014) Iron chelation by deferoxamine prevents renal interstitial fibrosis in mice with unilateral ureteral obstruction. *PloS one* **9**, e89355

63. Halliday, J. W., and Searle, J. (1996) Hepatic iron deposition in human disease and animal models. *Biometals* **9**, 205-209

64. Murphy, M. M., Lawson, J. A., Mathew, S. J., Hutcheson, D. A., and Kardon, G. (2011) Satellite cells, connective tissue fibroblasts and their interactions are crucial for muscle regeneration. *Development* **138**, 3625-3637

65. Sato, K., Li, Y., Foster, W., Fukushima, K., Badlani, N., Adachi, N., Usas, A., Fu, F. H., and Huard, J. (2003) Improvement of muscle healing through enhancement of muscle regeneration and prevention of fibrosis. *Muscle & nerve* **28**, 365-372

66. Li, Y., Foster, W., Deasy, B. M., Chan, Y., Prisk, V., Tang, Y., Cummins, J., and Huard, J. (2004) Transforming growth factor-beta1 induces the differentiation of myogenic cells into fibrotic cells in injured skeletal muscle: a key event in muscle fibrogenesis. *Am J Pathol* **164**, 1007-1019

67. Charge, S. B., and Rudnicki, M. A. (2004) Cellular and molecular regulation of muscle regeneration. *Physiol Rev* **84**, 209-238

68. Yoshida, T., Galvez, S., Tiwari, S., Rezk, B. M., Semprun-Prieto, L., Higashi, Y., Sukhanov, S., Yablonka-Reuveni, Z., and Delafontaine, P. (2013)

Angiotensin II inhibits satellite cell proliferation and prevents skeletal muscle regeneration. *J Biol Chem* **288**, 23823-23832

69. Lluis, F., Perdiguero, E., Nebreda, A. R., and Munoz-Canoves, P. (2006) Regulation of skeletal muscle gene expression by p38 MAP kinases. *Trends Cell Biol* **16**, 36-44

70. Wu, Z., Woodring, P. J., Bhakta, K. S., Tamura, K., Wen, F., Feramisco, J. R., Karin, M., Wang, J. Y., and Puri, P. L. (2000) p38 and extracellular signal-regulated kinases regulate the myogenic program at multiple steps. *Mol Cell Biol* **20**, 3951-3964

71. Sarbassov, D. D., Jones, L. G., and Peterson, C. A. (1997) Extracellular signal-regulated kinase-1 and -2 respond differently to mitogenic and differentiative signaling pathways in myoblasts. *Mol Endocrinol* **11**, 2038-2047

72. Gredinger, E., Gerber, A. N., Tamir, Y., Tapscott, S. J., and Bengal, E. (1998) Mitogen-activated protein kinase pathway is involved in the differentiation of muscle cells. *J Biol Chem* **273**, 10436-10444

73. Rommel, C., Clarke, B. A., Zimmermann, S., Nunez, L., Rossman, R., Reid, K., Moelling, K., Yancopoulos, G. D., and Glass, D. J. (1999) Differentiation stage-specific inhibition of the Raf-MEK-ERK pathway by Akt. *Science* **286**, 1738-1741

74. Jones, N. C., Fedorov, Y. V., Rosenthal, R. S., and Olwin, B. B. (2001) ERK1/2 is required for myoblast proliferation but is dispensable for muscle gene expression and cell fusion. *J Cell Physiol* **186**, 104-115

75. Ardite, E., Barbera, J. A., Roca, J., and Fernandez-Checa, J. C. (2004) Glutathione depletion impairs myogenic differentiation of murine skeletal muscle C2C12 cells through sustained NF-kappaB activation. *Am J Pathol* **165**, 719-728

76. Hansen, J. M., Klass, M., Harris, C., and Csete, M. (2007) A reducing redox environment promotes C2C12 myogenesis: implications for regeneration in aged muscle. *Cell Biol Int* **31**, 546-553

77. Sestili, P., Barbieri, E., Martinelli, C., Battistelli, M., Guescini, M., Vallorani, L., Casadei, L., D'Emilio, A., Falcieri, E., Piccoli, G., Agostini, D., Annibalini, G., Paolillo, M., Gioacchini, A. M., and Stocchi, V. (2009) Creatine

supplementation prevents the inhibition of myogenic differentiation in oxidatively injured C2C12 murine myoblasts. *Mol Nutr Food Res* **53**, 1187-1204

78. Buck, M., and Chojkier, M. (1996) Muscle wasting and dedifferentiation induced by oxidative stress in a murine model of cachexia is prevented by inhibitors of nitric oxide synthesis and antioxidants. *EMBO J* **15**, 1753-1765

79. Fulle, S., Protasi, F., Di Tano, G., Pietrangelo, T., Beltramin, A., Boncompagni, S., Vecchiet, L., and Fano, G. (2004) The contribution of reactive oxygen species to sarcopenia and muscle ageing. *Experimental gerontology* **39**, 17-24

80. Guttridge, D. C., Mayo, M. W., Madrid, L. V., Wang, C. Y., and Baldwin, A. S., Jr. (2000) NF-kappaB-induced loss of MyoD messenger RNA: possible role in muscle decay and cachexia. *Science* **289**, 2363-2366

81. Wang, H., Hertlein, E., Bakkar, N., Sun, H., Acharyya, S., Wang, J., Carathers, M., Davuluri, R., and Guttridge, D. C. (2007) NF-kappaB regulation of YY1 inhibits skeletal myogenesis through transcriptional silencing of myofibrillar genes. *Mol Cell Biol* **27**, 4374-4387

82. Powers, S. K., Duarte, J., Kavazis, A. N., and Talbert, E. E. (2010) Reactive oxygen species are signalling molecules for skeletal muscle adaptation. *Experimental physiology* **95**, 1-9

83. Kefaloyianni, E., Gaitanaki, C., and Beis, I. (2006) ERK1/2 and p38-MAPK signalling pathways, through MSK1, are involved in NF-kappaB transactivation during oxidative stress in skeletal myoblasts. *Cell Signal* **18**, 2238-2251

84. Barbieri, E., and Sestili, P. (2012) Reactive oxygen species in skeletal muscle signaling. *J Signal Transduct* **2012**, 982794

Figure legends

Fig 1. Iron content, oxidative stress, MAPKs phosphorylation, and satellite cell markers in mice models of aging, diabetes, and chronic kidney disease (CKD)

(A) Iron content of skeletal muscle in 2-month-old versus 2-year-old mice, *db/m* mice versus *db/db* mice, and control mice versus CKD mice. Values are expressed as mean ± SD. *$P < 0.05$ (in each paired comparison); n = 8 in each group. (B) Left panel: Representative images of DHE staining of skeletal muscle of 2-month-old versus 2-year-old mice, *db/m* mice versus *db/db* mice, and control mice versus CKD mice with negative controls in each mouse (NC: negative control). Right panel: Quantitative analysis of relative fluorescence intensity. Values are expressed as mean ± SD; n = 5 in each group. *$P < 0.05$ (in each paired comparison). (C) mRNA expression of the satellite cell markers *Pax-7*, *MyoD*, and *Myf5* in skeletal muscle of 2-month-old versus 2-year-old mice, *db/m* mice versus *db/db* mice, and control mice versus CKD mice. Values are expressed as mean ± SD; n = 5 in each group. *$P < 0.05$ (in each paired comparison). Phosphorylation of (D) p38MAPK and (E) ERK1/2 in skeletal muscle of 2-month-old versus 2-year-old mice, *db/m* mice versus *db/db* mice, and control mice versus CKD mice. Upper panel: representative protein expression levels of phosphorylated p38MAPK, total p38MAPK, phosphorylated ERK1/2, total ERK1/2, and tubulin. Lower panels: semi-quantitative densitometry analysis of p38MAPK and ERK1/2 phosphorylation. Values are expressed as mean ± SD. *$P < 0.05$ (in each paired comparison); n = 5 in each group.

Fig 2. Iron status, oxidative stress, MAPK phosphorylation, and satellite cell marker levels, and histology of skeletal muscle at basal conditions in mice with vehicle treatment or iron overload.

(A) Iron concentration in skeletal muscles. Values are expressed as mean ± SD. **$P <$ 0.01; n = 6–12 in each group. (B) Protein expression of H-ferritin (FTH) and L-ferritin (FTL) in skeletal muscle. Upper panel: representative protein expression levels of FTH, FTL, and tubulin. Lower panels: semi-quantitative densitometry analysis of FTH and FTL expression. Values are expressed as mean ± SD. **$P < 0.01$; n = 6–9 in each group. (C) Left panel: Representative images of DHE staining of skeletal muscle with negative controls in each mouse. Right panel: Quantitative analysis of relative fluorescence intensity. Values are expressed as mean ± SD; n = 6–9 in each group. **$P < 0.01$ (vs. vehicle). (D) Malondialdehyde concentration in skeletal muscle. Values are expressed as mean ± SD; n = 11–12 in each group. *$P < 0.05$. (E) mRNA expression of satellite cell markers in skeletal muscle. Values are expressed as mean ± SD; n = 10–14 in each group. **$P < 0.01$ (vs. vehicle). (F) Left panels: Representative images of Pax-7 (red), 4′,6-diamidino-2-phenylindole (DAPI, blue), and merged (purple) with negative control in gastrocnemius muscle of vehicle-treated and iron-treated mice. Right panel: Quantitative analysis of Pax-7 positive cells. Values are expressed as mean ± SD; n = 5-6 in each group. *$P < 0.05$ (vs. vehicle). (G) Left panel: Representative images of skeletal muscle with or without iron load. Right panel: The mean area of muscle fibers.

Values are expressed as mean ± SD. (H) mRNA expression of atrogen-1 and MuRF1 in skeletal muscle. Values are expressed as mean ± SD; n = 7 in each group. (I) Left panels: Representative images of RhoNox-1 (red), hydroxyphenyl fluorescein (HPF, green), 4′,6-diamidino-2-phenylindole (DAPI, blue), and merged (orange) with negative control in gastrocnemius muscle of vehicle-treated and iron-treated mice. Right panel: Semi-quantitative analysis of RhoNox-1 and HPF fluorescence intensity. Values are expressed as mean ± SD; n = 5 in each group. $*P < 0.05$ (vs. vehicle).

Fig 3. Regeneration of skeletal muscle after cardiotoxin (CTX)-induced injury in mice with or without iron treatment

(A) The effect of iron overload on the changes in *myogenin* and *Myh3(eMyh)* mRNA expression in skeletal muscle after CTX injection. Values are expressed as mean ± SD. $*P < 0.05$, $**P < 0.01$ (vs. vehicle at same day); n = 6-14 in each group. (B) Left; Representative images of CTX-induced muscle injury at day 7 with or without iron loading. Right; The percentage of regenerating myofibers with centralized nuclei, the mean area of muscle fibers, and the distribution of myofiber areas in skeletal muscles 7 days after CTX injection. Values are expressed as mean ± SD. $** P < 0.01$ (vs. vehicle); n = 6–14 in each group. (C) Left; Representative images of CTX-induced muscle injury at day 15 with or without iron loading. Right; Percentage of regenerating myofibers with centralized nuclei, the mean area of muscle fibers, and the distribution of myofiber areas in skeletal muscles at 15 days after CTX injection. Values are expressed as mean ± SD. $** P < 0.01$ (vs. vehicle); n = 5-6 in each group. (D) The effect of iron overload

on changes in *Collagen 1a1* (*Col1a1*), *Collagen 1a2* (*Col1a2*), and *Collagen III* (*Col3a1*), and *Transforming growth factor beta-1* (*Tgf-β1*) mRNA expression in skeletal muscle after CTX injection. Values are expressed as mean ± SD. *$P < 0.05$ (vs. vehicle at same day); n = 6 in each group. (E) Histological analysis of fibrosis in skeletal muscle at day 15 after CTX injury. Left; Representative images of picrosirius red staining in CTX-induced muscle injury at day 15 with or without iron loading. Right; Percentage of fibrosis fraction in skeletal muscles at 15 days after CTX injury. Values are expressed as mean ± SD. ** $P < 0.01$ (vs. vehicle); n = 5-6 in each group. (F) The effect of iron overload on the alteration in p38 and ERK1/2 phosphorylation in skeletal muscles after CTX injection. Values are expressed as mean ± SD. *$P < 0.05$, ** $P < 0.01$ (vs. vehicle at same day); n = 6-10 in each group.

Fig 4. Effect of iron on C2C12 myoblast differentiation

(A) Effect of iron on cell proliferation and death in C2C12 myoblast cells. Left: Myoblast proliferation with or without iron stimulation. Values are expressed as mean ± SD, n = 8 in each group. *$P < 0.05$, **$P < 0.01$. Right: Myoblast death with or without iron stimulation. Values are expressed as mean ± SD, n = 8 in each group. *$P < 0.05$. (B) Western blot images of myogenin, myosin heavy chain (Myh)3, FTH, FTL, and tubulin during myoblast differentiation. The changes in protein expression of myogenin and Myh3 with or without iron treatment during myoblast differentiation. Values are expressed as mean ± SD. *$P < 0.05$, ** $P < 0.01$; n = 16 in each group. (C) Effect of

iron on fusion index. Left: Representative immunohistochemical fluorescence of Myh3 (green) and DAPI (blue) in C2C12 myoblast cells. Right: Semi-quantitative analysis of fusion index. Values are expressed as mean ± SD. **$P < 0.01$; n = 7 in each group. (D) The effect of iron on the alteration of p38 and ERK1/2 phosphorylation during C2C12 myoblast differentiation. Values are expressed as mean ± SD. *$P < 0.05$, **$P < 0.01$; n = 7–8 in each group.

Fig 5. The effect of tempol on iron-mediated suppressive effect on C2C12 myoblast differentiation

(A) Iron content of C2C12 myoblast cells. Values are expressed as mean ± SD. *$P < 0.05$, ** $P < 0.01$; n = 6 in each group. (B) Iron-induced intracellular oxidative stress of C2C12 myoblast cells with or without tempol. Values are expressed as mean ± SD. ** $P < 0.01$; n = 12-18 in each group. (C) The effect of tempol on the suppression of muscle differentiation induced by iron. Values are expressed as mean ± SD. *$P < 0.05$, **$P < 0.01$ (vs. other 3 groups at same day); n = 12-16 in each group. (D) The effect of tempol on iron-mediated suppression of fusion index. Values are expressed as mean ± SD. *$P < 0.05$, **$P < 0.01$; n = 7 in each group. (E) The effect of tempol on iron-mediated reduction of p38MAPK and ERK1/2 phosphorylation. Values are expressed as mean ± SD. *$P < 0.05$, **$P < 0.01$ (vs. Fe+Tempol at same time); n = 8 in each group. (F) p38MAPK activity at 0 and 5 min after change in differentiation medium in C2C12 myoblast cells with or without iron treatment. Values are expressed as mean ± SD. *$P <$

0.05, **$P < 0.01$; n = 7 in each group. (G) p38MAPK activity at 5 min after change of

differentiated medium in iron-treated C2C12 myoblast cells with or without tempol.

Values are expressed as mean ± SD. *$P < 0.05$ (vs. Fe); n = 7 in each group.

Figure 1 Ikeda, et al.

Figure 1

(A)

Skeletal muscle iron content (µg Fe/g wet tissue)

* (2Y)
** (db/db)
** (CKD)

2M 2Y   db/m db/db   cont CKD

(B)

2M-NC | 2M
db/m-NC | db/m
cont-NC | cont
2Y-NC | 2Y
db/db-NC | db/db
CKD-NC | CKD
100µm

DHE fluorescence intensity (Relative fold change)

* (2Y)
** (db/db)
* (CKD)

2M 2Y   db/m db/db   cont CKD

(C)

Pax-7 mRNA (Relative fold change)

* (2Y) * (db/db) * (CKD)

2M 2Y   db/m db/db   cont CKD

MyoD mRNA (Relative fold change)

* (db/db) * (CKD)

2M 2Y   db/m db/db   cont CKD

Myf5 mRNA (Relative fold change)

* (2Y) * (db/db) * (CKD)

2M 2Y   db/m db/db   cont CKD

(D)

P-p38 — 48 / 48
T-p38 — 48
Tubulin — 48

2M 2Y   db/m db/db   cont CKD

P-p38MAPK protein (Relative fold change)

* (2Y) * (db/db) * (CKD)

2M 2Y   db/m db/db   cont CKD

(E)

P-ERK1/2 — 48
T-ERK1/2 — 48
Tubulin — 48

2M 2Y   db/m db/db   cont CKD

P-ERK1/2 protein (Relative fold change)

* (2Y) * (db/m) * (cont)

2M 2Y   db/m db/db   cont CKD

Figure 2 Ikeda, et al.

Figure 2-4

(A)

(B)

FTH — 20

FTL — 20

Tubulin — 48

Vehicle   Fe

(C)

DHE

Negative
control

Vehicle   Fe

100µm

(D)

(E)

(F)

1st Ab (-)   Pax-7   DAPI   Merge

Vehicle

Fe

100µm

Figure 2 continued

Figure 2-4

(G)

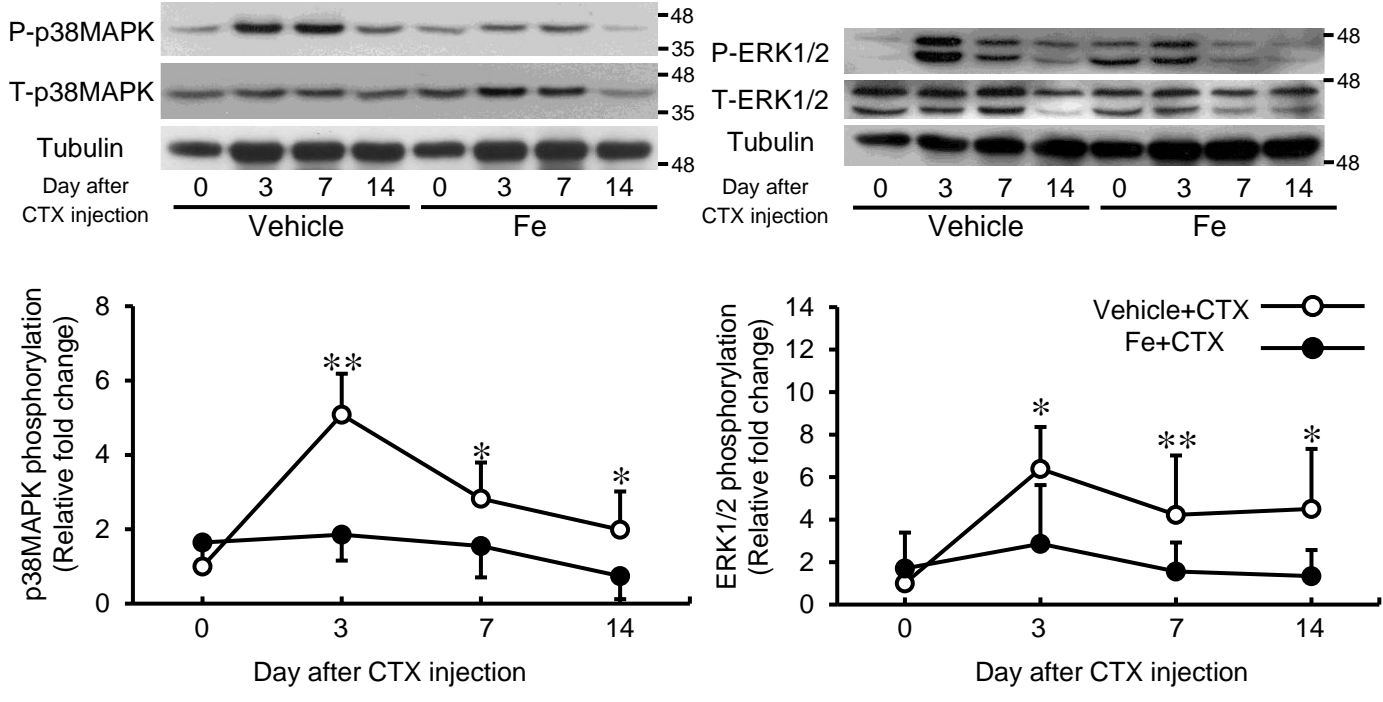
(H)

(I)

Figure 3 Ikeda, et al.

Figure 2-4

(A)

Vehicle+CTX ○
Fe+CTX ●

(B)

(C)

(D)

(E)

Vehicle+CTX day 15   Fe+CTX day 15

Figure 3 continued

Figure 2-4

(F)

Figure 4 Ikeda, et al.

Figure 2-4

(A)

(B)

(C)

100μm

(D)
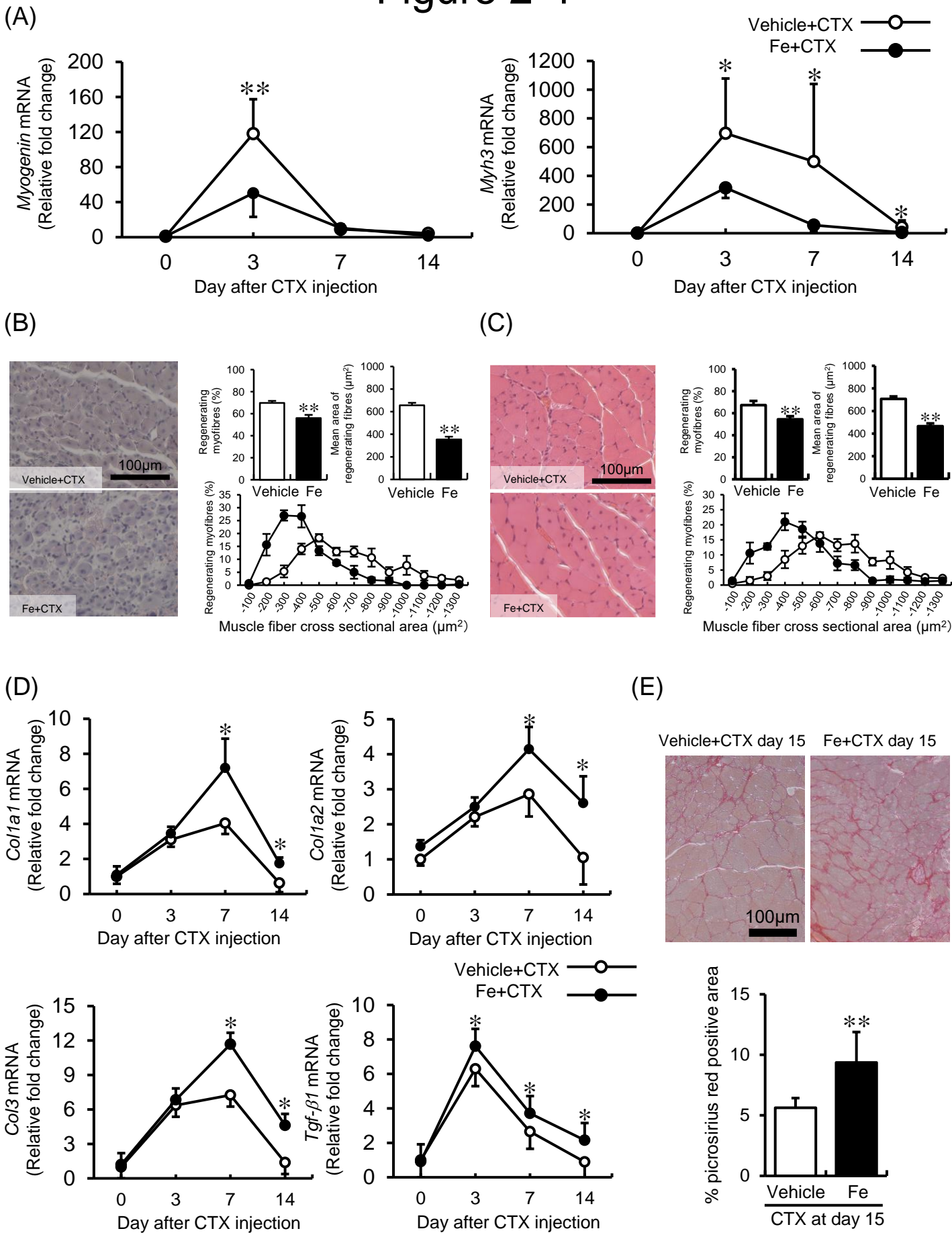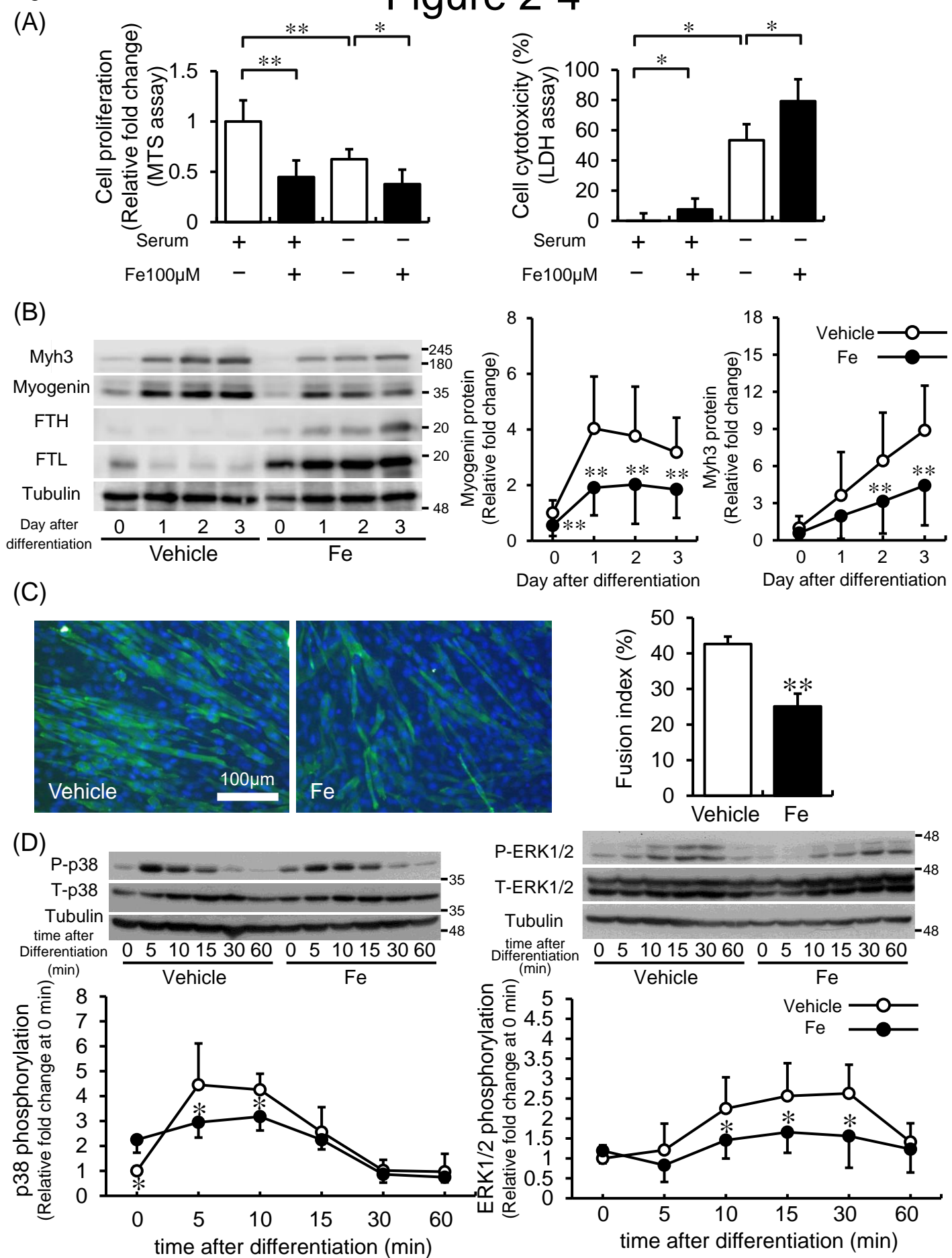
Figure 5 Ikeda, et al.

Figure 5
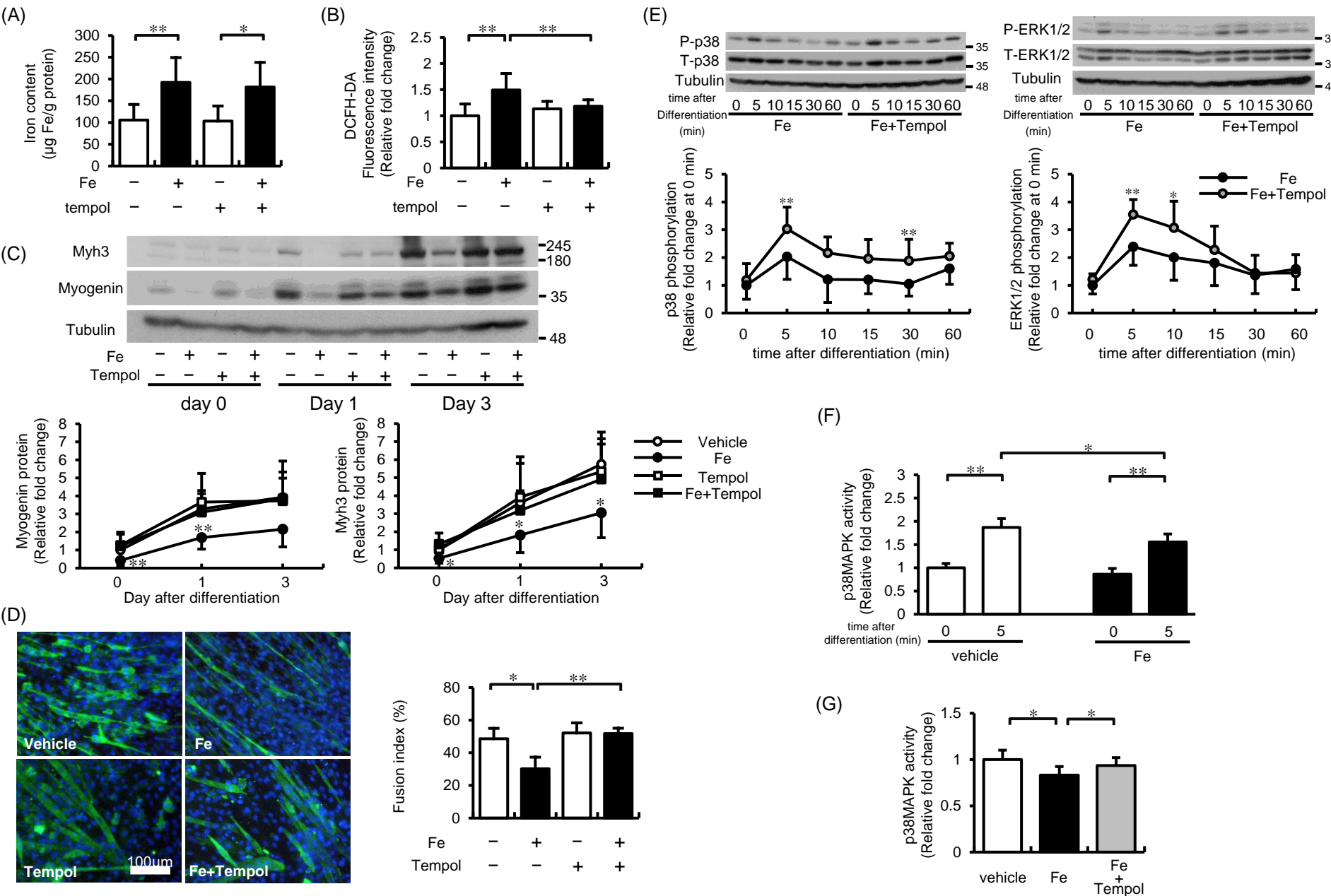
Table 1. Characteristics of vehicle-treated mice and chronic iron-treated mice

|	Vehicle-treated group	Iron-treated group
Initial body weight (g)	20.9 ± 1.3	20.9 ± 0.8
Body weight 4 weeks later (g)	24.9 ± 2.9	24.2 ± 1.5
Gastrocnemius muscles (mg)	141.2 ± 20.0	136.4 ± 8.9
Soleus muscles (mg)	9.2 ± 1.2	9.0 ± 1.3
Extensor digitorum longus muscles (mg)	14.4 ± 1.4	13.7 ± 0.9

Values are expressed as mean ± SD. n = 5-14 in each group.
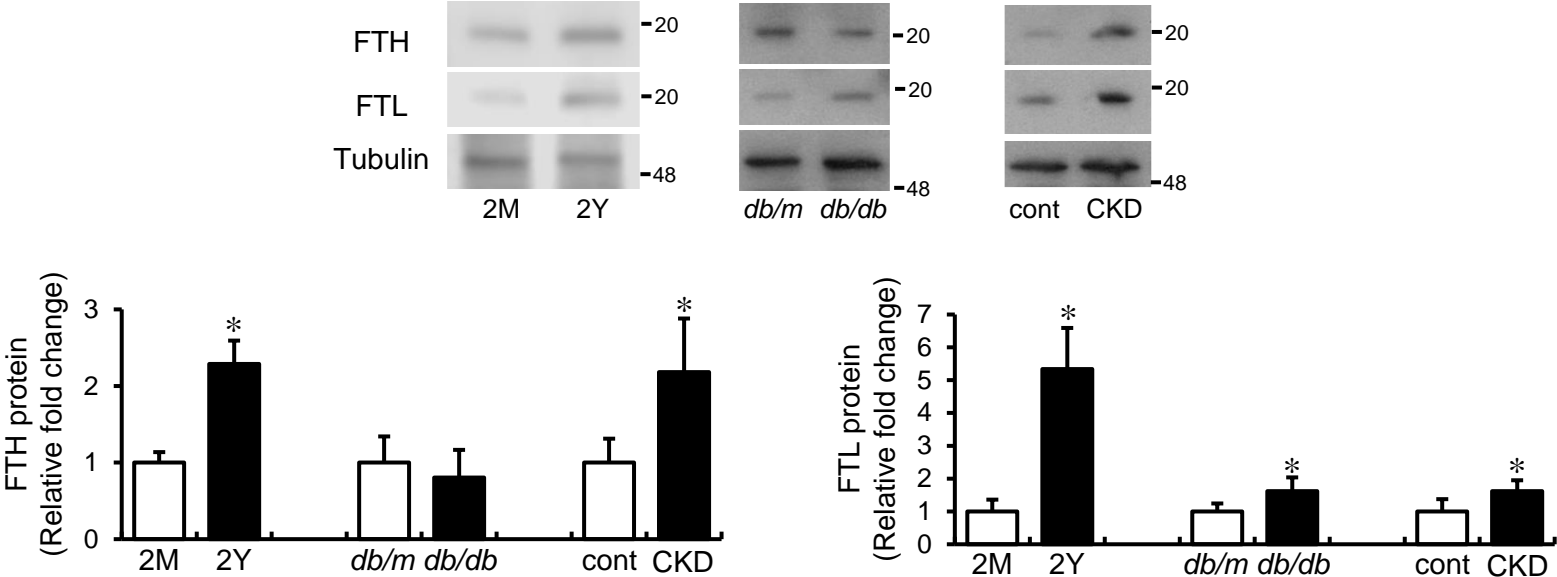
Supplementary figure 1

Protein expression of H-ferritin (FTH) and L-ferritin (FTL) in skeletal muscle of 2-month-old and 2-year-old mice, *db/m* mice and *db/db* mice, and control mice and CKD mice. Upper panel: representative protein expression levels of FTH, FTL, and tubulin. Lower panels: semi-quantitative densitometry analysis of FTH and FTL expression. Values are expressed as mean ± SD. *$P < 0.05$ (vs. 2 months of age, *db/m* mice, and control mice in each); n = 5 in each group.

(A)
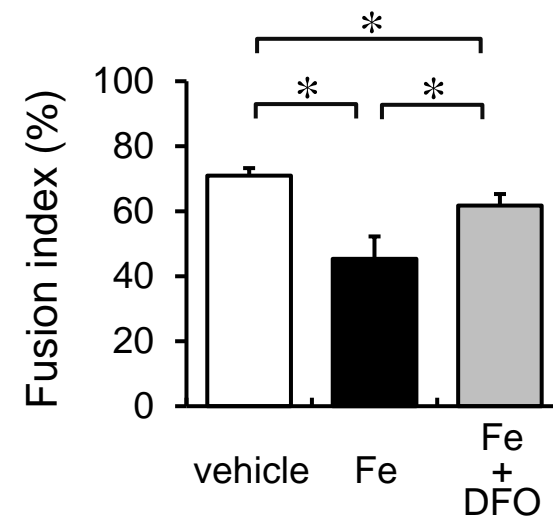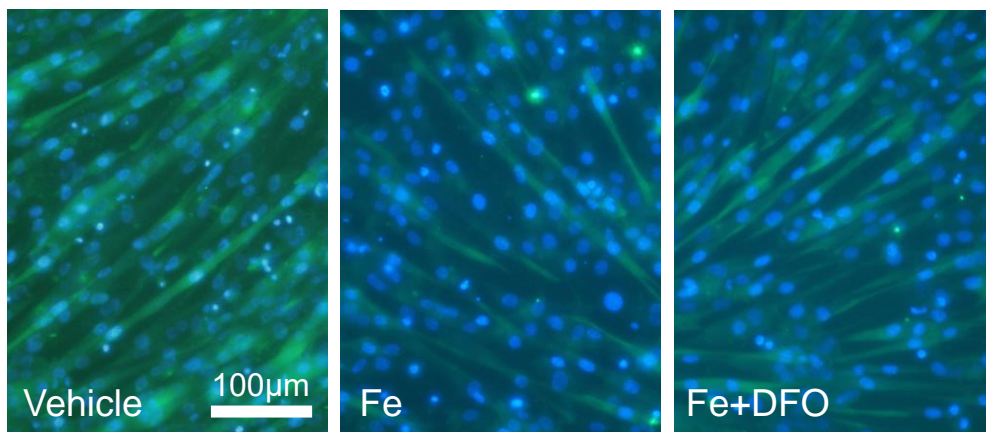
(B)
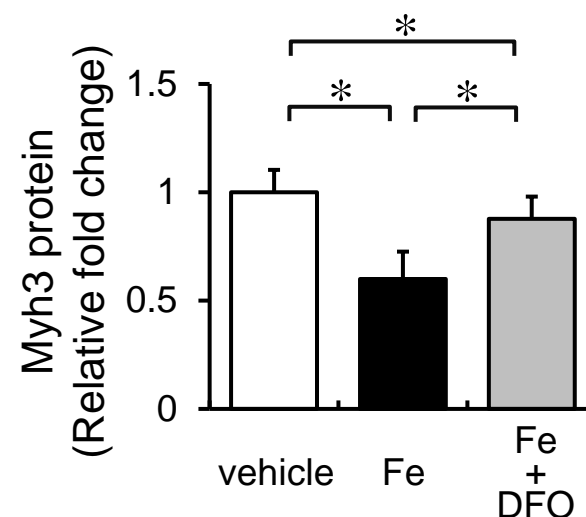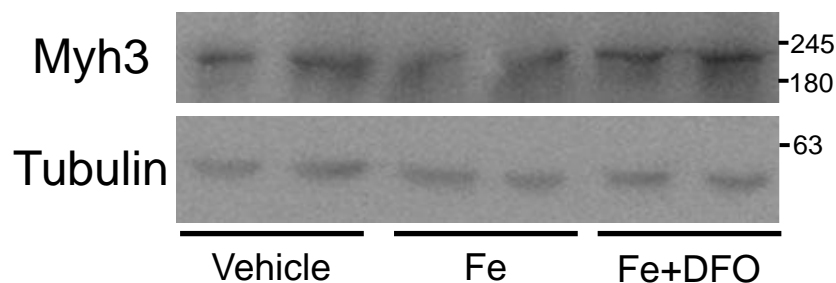
Supplementary figure 2

The effect of deferoxamine (DFO) on iron-mediated suppression of myoblast differentiation. (A) Effect of iron on fusion index. Left: Representative immunohistochemical fluorescence of Myh3 (green) and DAPI (blue) in C2C12 myoblast cells. Right: Semi-quantitative analysis of fusion index. Values are expressed as mean ± SD. *$P < 0.05$; n = 5 in each group. (B) Western blot images of myosin heavy chain (Myh)3, and tubulin during myoblast differentiation. Values are expressed as mean ± SD. *$P < 0.05$; n = 5 in each group.